# The evolution of deep convective systems and their associated cirrus outflows

George Horner[1] and Edward Gryspeerdt[1,2]

[1]Space and Atmospheric Physics Group, Imperial College London, London, UK
[2]Grantham Institute - Climate Change and the Environment, Imperial College London, London, UK

**Correspondence:** George Horner (g.horner20@imperial.ac.uk)

**Abstract.**

Tropical deep convective clouds, particularly their large cirrus outflows, play an important role in modulating the energy balance of the Earth's atmosphere. Whilst the cores of these deep convective clouds have a significant shortwave (SW) cooling effect, they dissipate quickly. Conversely, the thin cirrus that flow from these cores can persist for days after the core has dissipated, reaching hundreds of kilometers in extent. These thin cirrus have a potential for large warming in the tropics. Understanding the evolution of these clouds and how they change in response to anthropogenic emissions is therefore important to understand past and future climate change.

This work uses a novel approach to investigate the evolution of tropical convective clouds by introducing the concept of 'Time Since Convection' (TSC). This is used to build a composite picture of the lifecycle of deep convection, from anvil cirrus to thin detrained cirrus. Cloud properties are a strong function of time since convection, showing decreases in the optical thickness, cloud top height, and cloud fraction over time. After an initial dissipation of the convective core, changes in thin cirrus cloud amount were seen beyond 200 hours from convection.

Finally, in the initial stages of convection there was a large net negative cloud radiative effect (CRE). However, once the convective core had dissipated after 6-12 hours, the sign of the CRE flipped, and there was a sustained net warming CRE beyond 120 hours from the convective event. Changes are present in the cloud properties long after the main convective activities have dissipated, signalling the need to continue further analysis at longer time scales than previously studied.

## 1 Introduction

Deep convective clouds (DCC) occur primarily in the tropical and subtropical regions. They are characterized by one or more convective cores (cumulus towers), with strong updrafts that merge the cores at higher altitudes and large anvils flowing out from the region of convection (Fan et al., 2013). The radiative forcing from deep convective cores in the tropics can vary greatly depending on the optical thickness and ice water path of the cloud (Berry and Mace, 2014; Hartmann and Berry, 2017). However, the overall total cloud radiative effect (CRE) in the tropics is small (Wielicki et al., 1996). This is due to the cancellation of the large (longwave) LW warming that occurs in cloudy regions in the tropics, and the significant SW CRE that

comes from the high albedo of these same regions. This leads to the CRE in cloudy regions of the tropics being very similar to
25    the CRE in nearby non-convective regions (Hartmann and Berry, 2017; Harrison et al., 1990; Ramanathan et al., 1989).

Whether this cancellation is due to feedbacks or is simply a coincidence is unclear (Kiehl, 1994; Hartmann et al., 2001b).
If a coincidence, then the behaviour of these deep convective regimes may change in a warming world, or under different
aerosol concentrations. This cancellation is the sum of large SW and LW components. Therefore any small change in either
of these components could potentially have a large effect on the overall CRE. Understanding the lifecycle and drivers of deep
30    convection is thus important to understand the sensitivity of these regimes.

Whilst the convective cores alone have a negative CRE, their lifetimes are relatively short in comparison to the outflowing
anvil cirrus. Hartmann et al. (2001b) found that the TOA radiative forcing of DCC ranged between +20 to -119 Wm$^{-2}$, with
the optical depth of tropical DCC ranging from 1 to 60 in the upper troposphere. On the other hand, the detrained thin cirrus
from the anvil of the top of convective core can persist up to 5 days (Luo and Rossow, 2004), cover large spatial extents and
35    have a significant warming contribution to the CRE (Protopapadaki et al., 2017; Wall et al., 2018).

The sign of the radiative forcing from cirrus in the tropics is highly dependent on the optical thickness of the cloud ($\tau_c$).
Choi and Ho (2006) found that thin cirrus between 10-12km with an optical depth $\tau_c < 10$ have a warming effect, whilst cirrus
with $\tau_c > 10$ have a cooling effect. Koren et al. (2010) showed that the cloud top height also plays a vital role in the sign of the
forcing from cirrus. They showed that if the cirrus cloud top height is increased and optical depth decreased, there is potential
40    for much greater warming.

The lifecycle of deep convective and their associated anvil and thin cirrus outflows has been investigated in numerous prior
works, both in observations and models. Using observational data, Luo and Rossow (2004) found that 50% of of tropical
cirrus clouds originated from convection. They found that the detrained cirrus had, on average, longer lifetimes than the in-situ
cirrus, at around 30 hours compared to 19 hours for in-situ. This suggests some mechanism for sustaining water vapour at the
45    detrained cirrus height that allows for the longer lifetimes. Using ground based data and satellites, Mace et al. (2006) found
that 47% of cirrus observed over Manus island in the western Pacific originated from deep convection occurring within the
past 12 hours. Many other modelling and observational studies also show that at least 50% of tropical cirrus originate from
convection (Massie et al., 2002; Gehlot and Quaas, 2012; Riihimaki et al., 2012). Salathé and Hartmann (1997) showed that
upper tropospheric humidity is sustained for up to 5 days from convection. This is consistent with the cirrus decay found by
50    Luo and Rossow (2004).

Garrett et al. (2005) looked at the detailed evolution of a single thunderstorm anvil cirrus cloud in Florida. They found that
the advected outflow was separated into two cloud layers; a cirrus anvil at -45°C lying below a thin tropopause cirrus (TCC)
at -70°C. The TCC lifetime was sustained longer than that of the anvil cirrus, potentially due to anvil cirrus shielding the
TCC from terrestrial radiation, as proposed by Hartmann et al. (2001a). For a complete overview of the different cirrus types
55    and their origin, Krämer et al. (2016) synthesised multiple field campaigns, simulations and model results looking at cirrus
microphysics, splitting up in situ, detrained, liquid origin, and TTL cirrus.

Studies investigating the model evolution of cirrus found broadly similar results to those found in observations. Gehlot and
Quaas (2012) saw a rapid decay (6-12hrs) of deep convection from the peak, and an associated growth of cirrus in the ECHAM5

model. After one day they found a decay of the cirrostratus, likely associated with a loss of cloud water due to larger particles
that have a large sedimentation mass flux. Jensen et al. (2018) investigated the detrainment of ice crystals from the tops of deep
convection in a cloud resolving model (CRM). They found that most large ice crystals ($>200\mu$m in diameter) fall out of the
anvils within 2 hours of formation. The cirrus decay was much slower, occurring over 120 hours, from a maximum cirrus cloud
fraction of 0.4 to 0.15 after 120 hours. They also looked at changes under increased SSTs, finding anvil cirrus clouds having
increased cloud fractions, and higher cloud tops, leading to a positive cloud feedback.

Looking at the CRE of the evolution of the convective system, it is the balance between the LW and SW over the entire
lifetime of the cirrus in the tropics that, if perturbed, could lead to large changes in the overall net CRE. Most tropical radiative
studies are confined to models. Looking at the CRE along Lagrangian trajectories in simulation, Gasparini et al. (2021) found
that large SW and LW values dominate close to convection as expected. The net CRE oscillates close to zero and is a function
of the solar insolation. In their simulations most convection occurs in the early morning, there is a peak in net negative CRE at
peak solar insolation when SW cooling dominates. There is a slight warming at 15 hours, when the anvil has thinned sufficiently
and the solar insolation decreased enough for the LW CRE to dominate.

The factors that control the radiative evolution of the decaying cirrus have also been investigated in model studies. Gasparini
et al. (2019) found that at high ($>100$gm$^{-2}$) IWP values, or above the 80th percentile, the net CRE is negative. Beyond this,
at low IWP and correspondingly low cloud fractions above 12km the net CRE switches signs to a small positive value. This
switch occurs when the $\tau_c$ is around 4, roughly where precipitation stops occurring. This is a lower value for the $\tau_c$ than found in
observations by Choi and Ho (2006). As the CF and IWP decrease, the CRE tends to zero. The switch from warming to cooling
happens at around 6 hours from convection in Gasparini et al. (2019). They generally found that small scale microphysical and
dynamical processes are responsible for determining the lifecycle of the detrained anvil cloud. Current GCMs have too coarse
horizontal and vertical resolutions to accurately reflect the dynamical processes controlling anvil cirrus evolution (Wall and
Hartmann, 2018).

Most previous work focused on individual mesoscale studies and capped the analysis at shorter time scales in the region
of 120 hours. In contrast, this paper presents a method to run a Lagrangian trajectory analysis across the entire tropics at
unbounded trajectory lengths at a low computational cost, leading to changes being found in the cloud properties at time
scales far beyond 120 hours after the initial convection has dissipated. Used in conjunction with lidar and radar data, the
vertical evolution of the cloud properties are characterised as a function of time since convection.This paper's approach builds
a composite picture of the lifecycle tropical convective into thin cirrus.

## 2 Method

### 2.1 Data

Observational data from the 3-hourly ISCCP-H dataset at 1x1° from NOAA/NCEI is used to define locations of deep convection
(Rossow et al., 2017). ECMWF ERA5 reanalysis wind fields are used in the trajectory analysis (Hersbach et al., 2018) and to
characterise cloud properties. To examine the evolution of the radiative properties, the CERES SYN1deg L3 LW and SW TOA

| Regime | CTP / hPa | $\tau_c$ | CF / % |
|---|---|---|---|
| **Deep convective cores** | **242.6** | **10.5** | **99.5** |
| Mid latitude storm | 433.6 | 10.4 | 99.2 |
| Thin high cirrus | 316.3 | 1.2 | 79.9 |
| Polar | 395.6 | 2.2 | 84.5 |
| Middle top clouds | 606.9 | 9.5 | 97.2 |
| Fair weather | 645.1 | 3.2 | 40.0 |
| Shallow cumulus | 840.1 | 4.0 | 79.6 |
| Stratocumulus | 725.5 | 6.3 | 90.7 |

**Table 1.** ISCCP-H cloud regime centroid values for the CTP, $\tau_c$, and CF from Tselioudis et al. (2021). The deep convective cloud regime, DCC, is highlighted in bold.

fluxes are used (NASA/LARC/SD/ASDC, 2017). The vertical evolution of the cloud is investigated by utilising the DARDAR dataset, which is an ice cloud retrieval product that combines measurements from the CloudSAT radar and CALIPSO lidar (Delanoë and Hogan, 2008; Sourdeval et al., 2018). The period of study in this paper is 2008-2010 inclusive.

## 2.2 Convective core identification

In order to track the time since a parcel of air last experienced convection, convective cores were defined and identified in the satellite data. This work uses the 3-hourly ISCCP-H global weather states at 1x1° as defined using a regime analysis in Tselioudis et al. (2021). The ISCCP-H dataset is then separated into seven distinct cloud regimes using a nearest neighbours algorithm. These cloud regimes, and their associated centroid values, are shown in Table 1.

For a full description of the ISCCP-H weather states, see Tselioudis et al. (2021). This study is focused on the tropical region of 30S-30N and only considers the deep convection defined within the tropics, whereas the weather states in Table 1 are defined globally.

Subsequent conditions are applied to isolate the convective cores such that they have a $\tau_c > 8.5$ (albedo > 0.5) and a cloud top temperature (CTT) < 220K. The albedo is calculated from the optical thickness using Eq. 1.

$$\alpha = \frac{\tau_c^{0.895}}{\tau_c^{0.895} + 6.82} \tag{1}$$

as defined in the ISCCP simulator. Only the very brightest, thickest cores of the convective clouds are categorised as DCC. If these conditions aren't imposed then thick anvil cirrus are included as part of the convective cores, and the ability to investigate their temporal development is reduced.

The mean relative frequency of occurrence (RFO) for the convective cores for the years 2007-10 is shown in Fig. 1. Most of the convection occurs in the Maritime Continent, over Central Africa, South America, and along the ITCZ. This work is only concerned with tropical convection, defined in the region between the red boundaries (30S-30N).
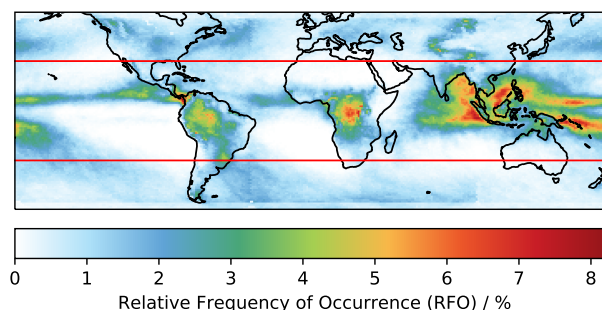
**Figure 1.** Relative frequency of occurrence (RFO) of the convective core regime from between 2007-2010. Red bands show the boundaries of the tropics (30S-30N).
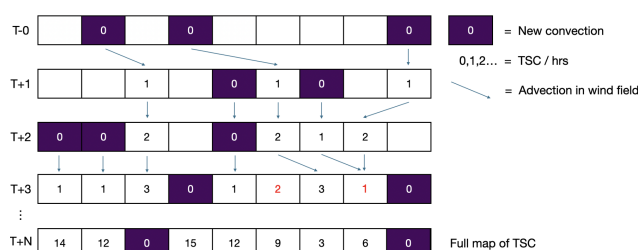
**Figure 2.** Schematic diagram of the advection process in one dimension, assuming all locations start with no TSC value. Red values indicate where either a divergence or convergence of pixels occurs. The purple boxes show new convection occuring, and the arrows highlight the advection of convective air into new gridboxes between timesteps. The values of the TSC are shown in each box.

## 2.3 Langrangian forward trajectories

The ECMWF ERA5 reanalysis wind speeds at 0.25° are used in this study (Hersbach et al., 2018). A pressure averaged wind field between 200hPa and 300hPa is used to advect the convective cores forward, in order to best reflect the range of heights that the convective cores and subsequent detrained cirrus exist. This is the same logic as applied in Luo and Rossow (2004), where vertical movement of air is not considered, however they use a pressure averaged wind field between 200hPa and 500hPa. The decision to use a higher altitude average wind field is addressed in section 2.5.

The advection process is as follows. All the points on the map are advected forward one hour in time according to the wind field. The TSC now has values of T+1 hours since convection. In locations where DCC are present, the TSC is reset to zero. This advection process repeats, each time resetting locations of DCC to zero TSC. Fig. 2 show a schematic diagram of the process in one dimension.

The TSC algorithm runs at 0.1x0.1° resolution. This is necessary to ensure that between one hour timesteps there is a high enough resolution so that parcels are advected out of the gridbox they currently occupy. If the algorithm was run at 1x1°, then the air would very rarely travel out of the gridbox that it occupies. For this reason, the resolution of the DCC dataset has to be

125  increased to 0.1x0.1° to be compatible with the TSC algorithm. The resolution of the outputted TSC files is averaged to 1x1°, a high enough resolution for subsequent analysis.

The TSC array is interpolated into missing regions after each advection timestep (Fig. 2). When each 0.1x0.1° pixel in the TSC array is advected forward, some of the pixels converge to occupy the same gridbox, necessarily leaving some gridboxes without a TSC value. When this occurs, the missing values are interpolated based on the TSC values around this empty gridbox.

130  Between each timestep, approximately 5% of the gridboxes are empty. When two trajectories enter the same gridbox, they will proceed to follow the same trajectory ad infinitum due to the deterministic nature of the trajectories. Therefore the trajectory with the smaller TSC value is the one that determines the TSC value at that gridbox from that point on. This ensures that any high TSC value really represents air at such long timescales since convection.

The TSC map is defined between 32S-32N to ensure that air is allowed to briefly leave the region of analysis and reenter.

135  If the wind field brings air from outside 32S-32N into this region, they will be given NaN values until new convection or advection replaces them. This increases confidence in the high TSC regions. If the TSC map is defined well beyond the tropics, the extratropics act like a reservoir of very high TSC values that are advected into the tropics. This inflates the TSC values, because no convection is defined outside of 30S-30N.

Since the map starts at zero TSC, there is an associated spin up time until every point on the map is a true reflection of the

140  hours since the air at that location last experienced convection. This spin up time is shown in Fig. 3 and is approximately 20 days. Therefore in all further analysis, the first mont of data are excluded.

## 2.4  Evaluation of TSC

After the spin up, there is minimal variability in the TSC across two years of data, with the mean TSC oscillating around 180 hours (Fig. 3). The 10th percentile is very consistent, due to the regularity of new convection occurring in the dataset. The 90th

145  percentile is more erratic, oscillating between 350 hours and occasionally over 500 hours, due to the sporadic nature of the occurrence of very high TSC regions and the long tail on the distribution of TSC.

It is interesting to note that the 90th percentile TSC values are considerably higher than the temporal length of the trajectories in prior works (Gehlot and Quaas, 2012; Luo and Rossow, 2004), which limit their analysis to 120 hours (5 days). This is a benefit of the TSC approach, which allows the trajectories to be advected as far as possible, so do not bias towards lower

150  trajectory values.

## 2.5  Comparison with HYSPLIT trajectories

A comparison can be made to individual trajectories initiated from locations of convection. The HYSPLIT Lagrangian forward trajectory model is used in this paper (Rolph et al., 2017). The HYSPLIT model uses reanalysis data from NCEP/NCAR to advect individual air parcels in a 3D wind field, which includes vertical transport of the air parcel. In this work, HYSPLIT

155  trajectories are initiated from the centre of each 1x1° box that contains a TSC-0 value, at an altitude of 10km. This altitude is between approximately 300hPa in the tropics. These trajectories are followed for 315 hours, with the TSC time at the location of each trajectory compared the time since the HYSPLIT trajectories were initiated. This is done for three times across 2008
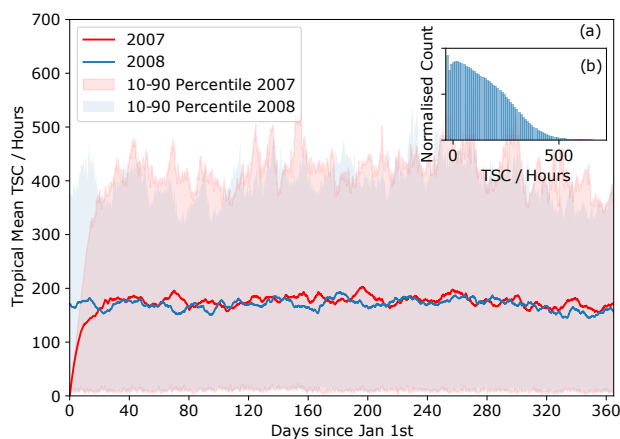
**Figure 3.** Tropical mean Time Since Convection (TSC) for 2007 and 2008, with 10th-90th percentiles highlighted. The top right histogram shows the normalised distribution of TSC values over the 2 year period, excluding the spin up time. There is little variation in the mean TSC between the years after the initial spin up period in 2007.
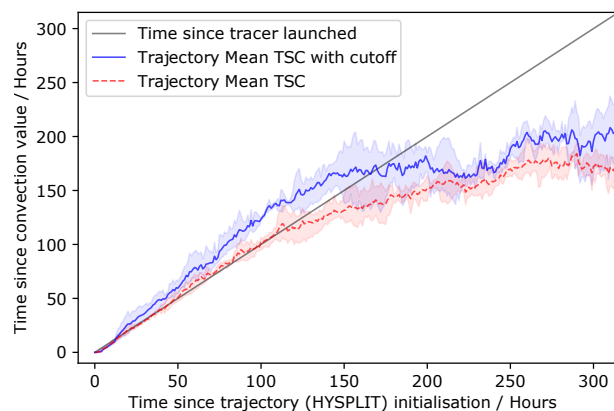
**Figure 4.** Median TSC values (y-axis) along HYSPLIT trajectories (x-axis), for all trajectories and for trajectories that are stopped once they reach new convection. Error range between maximum to minimum trajectory values. Straight line indicates an exact relationship between trajectory age and TSC value.

(Jan 1st, Jun 1st, and Sept 1st). Fig. 4 shows the median value of the TSC for the gridbox occupied by the trajectories. The dotted red line indicates all the trajectories initiated from the convective cores (1033 in total), whilst the solid blue line only includes trajectories up to the point at which they next experience convection, which better represents the values of the TSC methodology.

The TSC value and HYSPLIT value broadly match for lower TSC values (Fig. 4). However, particularly for the trajectories that stop when they experience new convection, the TSC values are higher than the time since the trajectories are initiated. The main reason for this difference is there is no vertical transport in the TSC advection algorithm. Rather, the average wind speeds between 200hPa-300hPa are used to advect the air parcels. The trajectories in the NCEP/NCAR HYSPLIT model are initiated at 10km, which in the tropics is an average pressure of 300hPa. This is lower than the average cloud top height of the convective cores in the TSC datatset. This height is an approximation of the DCC detrainment altitude, which leads to some uncertainty in the relevant wind level for advection. During the early stages of the HYSPLIT trajectory, the wind speed will be greater than in the TSC trajectory. This is because the HYSPLIT trajectory is at 200hPa and the TSC trajectory wind speed is averaged between the 200hPa and 300hPa wind speeds.

This explains why the TSC is greater than the age of the trajectories, as the HYSPLIT trajectories will move further from convection than modelled by the TSC dataset. As the trajectories subside (it is worth noting that there is uncertainty in the appropriate subsidence rate), the horizontal wind speeds decrease, and start to become closer to the wind speeds in the TSC dataset, therefore the difference between the age of the trajectories and the TSC becomes constant. As the trajectories begin to subside even more, the TSC values become closer to the age of the trajectories, until at around 150 hours where the TSC value becomes lower than the age of the trajectories. For this reason, it is suitable to use the 200-300hPa pressure levels, as they still best reflect the range of heights that the convective cores and subsequent cirrus exist at. This also reflects the decision to use these pressure levels over those used by Luo and Rossow (2004).

## 2.6 Cloud Properties

The ISCCP-H dataset is used to investigate how the CTP and $\tau_c$ change as a function of TSC. The change in the distribution of cloud properties from the ISCCP-H dataset as a function of TSC are shown in joint histograms. These histograms are limited to show the evolution of the tropical gridbox mean values for the region between 30S-30N.

Using the joint histograms, the $\tau_c$ and CTP of just the highest clouds that occupy the top 3 CTP bins (>375hPa) are isolated. This is done by multiplying the centroid value of the top 3 CTP bins by the cloud fraction of each bin from the joint histograms. This allows for a comparison for the evolution of the $\tau_c$ and CTP for all clouds, and just the highest clouds in the tropics.

When there are failed retrievals in the ISCCP-H dataset, it assigns that gridbox to the lowest $\tau_c$ and CTP bin in the joint histogram. These missing values significantly affect the high cloud $\tau_c$ and CTP, so are removed when generating the $\tau_c$ and CTP histograms.

The vertical evolution of the cirrus is investigated using the DARDAR dataset, a combination of the CloudSAT radar and CALIPSO lidar. The overpass locations of DARDAR are matched within the hour to the TSC at that location, at 1x1 degree resolution. The DARDAR cloud mask is used to filter out aerosol, ground, and unknown retrievals.
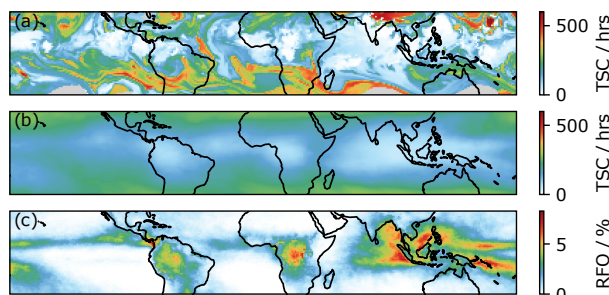
**Figure 5.** a) Snapshot of the TSC 30S-30N at 00:30UTC 26th July 2008. b) Mean TSC for between 2008-2010. c) RFO of deep convection between 2008-2010 (as in Fig. 1).

The radiative evolution of convection, from thick convective core to thin anvil cirrus, is investigated by analysing the CERES SYN1deg L3 LW and SW TOA fluxes (NASA/LARC/SD/ASDC, 2017). The CRE is calculated as the all sky minus clear sky radiative fluxes from the CERES data. In order to only look at the radiative evolution of the highest clouds, regions where the cloud fraction of the low clouds (as defined by the ISCCP joint histograms) is less than 1% is classified as high cloud gridboxes only. For the cloudiest regions in the tropics (which are also the regions of the lowest time since convection), there is often no hourly outgoing clear sky LW data. For these gridboxes, the 3 monthly seasonal average outgoing clear sky LW for these gridboxes is used, in order to calculate a value for the CRE.

The ISCCP histograms used to isolate the high clouds are only available during daylight, therefore the LW forcing is only available during daylight. The SW is known to be zero during the night, so the nighttime values for the SW are included in the analysis, even when there are no corresponding LW values. This assumes that the daytime LW values are representative of the nighttime values

## 3 Results

### 3.1 Regional distribution of Time Since Convection.

Fig. 5 shows the map of time since convection for the tropical region 30S-30N at 00:30 UTC on Jan 1st 2008.

As might be expected, the TSC map broadly follows the geographical distribution of the deep convective cores shown in Fig. 1. The areas of low TSC, such as the Maritime Continent and South America and Central Africa align with the regions of high DCC occurrence. However the low TSC regions are more spread out around the regions of DCC occurrence, as they are advected via the wind field away from the initial DCC. Regions of particularly high TSC are the extra tropical regions around 30S and 30N latitudes, far from convection.

## 3.2 Evolution of ISCCP cloud properties

As the optically thick deep convective cores dissipate, a reduction in the cloud optical thickness ($\tau_c$) is expected, as the anvil cirrus decays into thin cirrus and eventually disappears completely. Changes in the cloud top pressure (CTP) are also expected, moving from low pressure (high altitude) close to the convective core, to higher pressures (lower altitude) as the anvil cirrus

215  extends and sinks (Luo and Rossow, 2004).

Fig. 6 shows the ISCCP-H joint histograms in the first 5 days since convection, with each 24 hour period showing the joint histogram of CTP and $\tau_c$. At Day-0 (0<TSC<24) the histogram is dominated by optically thick, high altitude clouds, with high cloud fractions. There is very little low cloud, which may be due to the thick high cloud obscuring the clouds below them. However, low clouds become visible in the first 24 hours since convection. There is a shift to optically thin clouds as

220  TSC increases. This implies that the thick anvil cirrus clouds do not persist longer than 24 hours post convection, consistent with previous studies by Luo and Rossow (2004). This is supported by Fig. 6, showing the difference is largest between day 0 and day 1 than any subsequent day. High clouds with an optical thickness in the middle two bins (between 2.3 and 14.5) still noticeably persist up to day 5, representing the thicker cirrus outflow, with the most significant decrease in their cloud fraction happening 3 days after convection. They remain with low cloud fractions up to day 25.

225  From day 4 onwards, low clouds begin to dominate in the joint histogram, however there is still a presence of thin cirrus. Interestingly, small changes in the cloud fractions are still seen between day 10 and day 15, particularly an increase in low cloud and decrease in high cloud. This implies that the TSC is still relevant at up to 360 hours from convection. Note that the top left bin remains particularly high across all histograms. This is due to the failed retrievals which can't be assigned into a particular $\tau_c$/CTP bin which by default are are assigned into top left bin in the ISCCP-H dataset (Pincus et al., 2012), as

230  mentioned in section 2.6.

These results are generally consistent with previous work (Gehlot and Quaas, 2012; Luo and Rossow, 2004), however this paper sees a slightly quicker decay of the anvil cirrus than in Luo and Rossow (2004), and continued changes in cloud fraction beyond 5 days from convection.

Luo and Rossow (2004) also use a column averaged wind field between 200hPa-500hPa, whereas this work uses 200hPa-

235  300hPa to better reflect the range of heights at which the anvil cirrus and detrained thin cirrus occur at. The wind field in this work will be on average faster than Luo and Rossow (2004), and therefore the air will travel further in the same period of time. As such a TSC value of 10 hours will be geographically further along the trajectory than in Luo and Rossow (2004). This will cause the lifetime of the convective outflow clouds to appear shorter in this work.

Seeing changes in the cloud fraction at such long TSC values is a consequence of the approach of this work. Unlike previous

240  studies, where the trajectories were stopped at predetermined times, this work tracks air from convection for an unbounded amount of time. Therefore changes in cloud properties can be tracked at much longer times since convection than previous work, without having to pick out specific convective events that are known to reach a certain age, and also deals with scenarios in which a trajectory is overlapped by new convection.
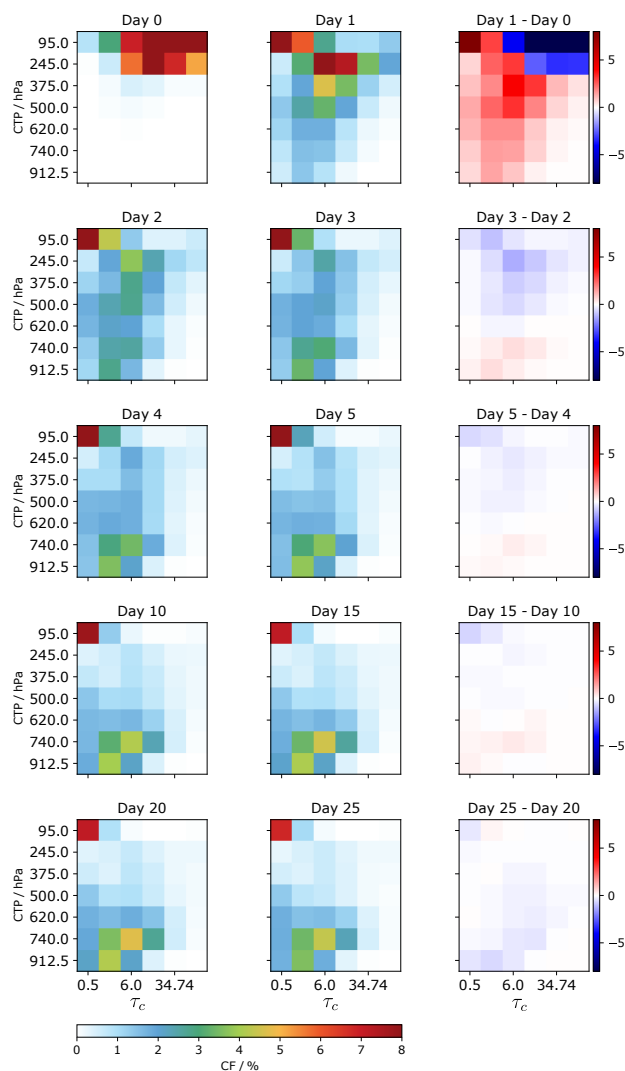
**Figure 6.** ISCCP-H joint histograms showing the distribution of the CTP, and $\tau_c$ and cloud fraction as a function of days since convection. The rightmost column shows the absolute percentage change between days. Day 0 is the first 0-24 hours since convection, day 1 is 24-48 hours since convection, and so on. High CF values for upper right gridboxes would indicate a distribution skewed towards optically thick, high altitude clouds, and the opposite (optically thin, low altitude), for bottom left.
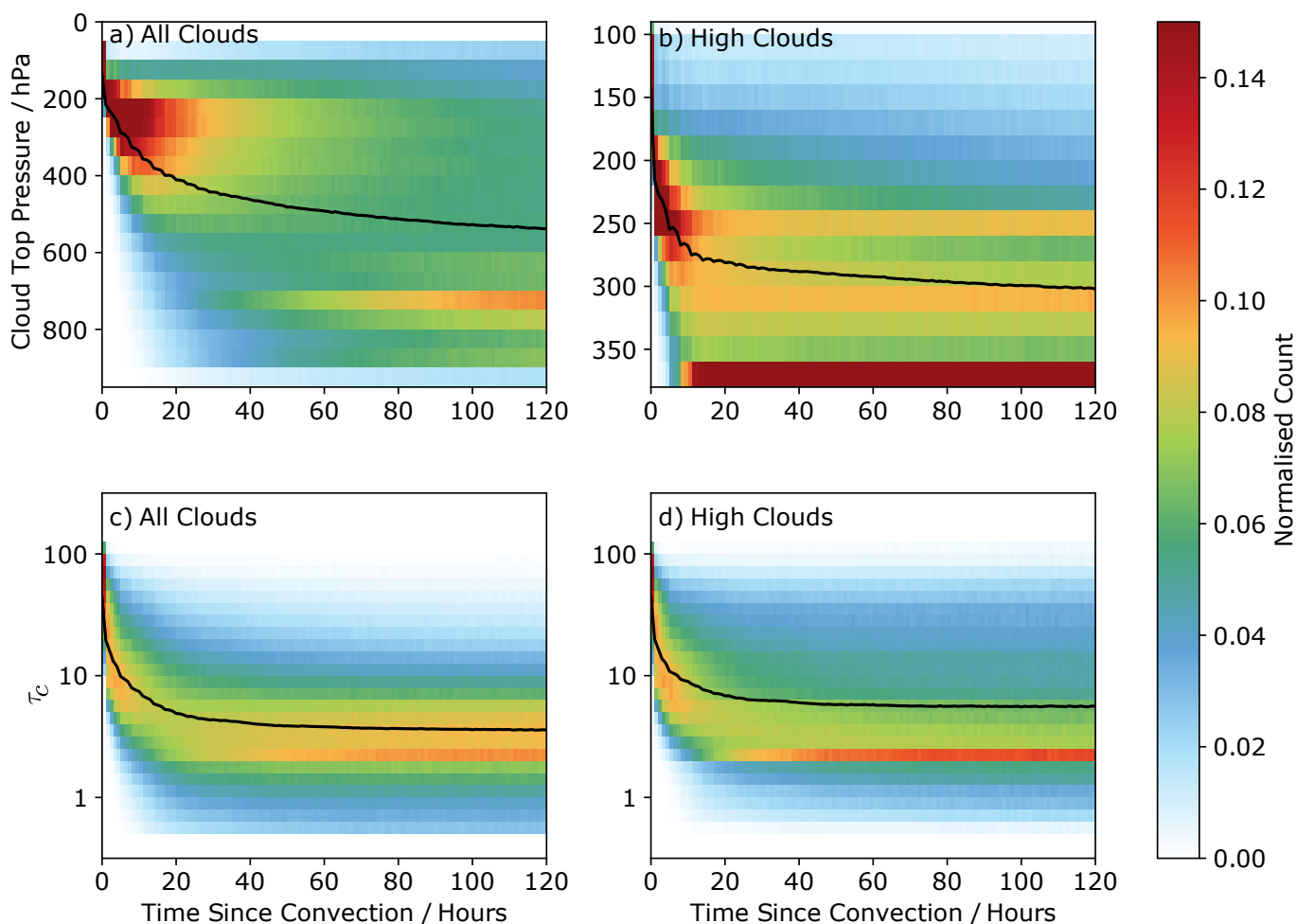
**Figure 7.** ISCCP cloud properties as a function of TSC. The normalised distribution represents the probability of finding clouds with a particular CTP or $\tau_c$ for a given TSC value. The black line indicates the mean value. Left-hand column shows the CTP and $\tau_c$ for all clouds, and right-hand column for high clouds only.

### 3.3 Evolution of cloud properties

245 Fig. 7 shows the evolution of the CTP and $\tau_c$ respectively as a function of the TSC for both all cloud pixels (Fig. 7a,b) and the high cloud only pixels (Fig. 7c,d). The joint histograms are normalised so that the number of y-axis bins add up to unity, to account for the fact that there are more retrievals for smaller TSC values. This provides a higher temporal resolution than the histograms in Fig. 6.

Fig. 7a shows that the CTP initially sits at very high altitudes for the convective cores, around 200hPa, coincident with the

250    upper level wind field used. There is a quick decay in the mean CTP in the first day since convection, as the convective core thins, and the mean CTP is skewed by the optically thicker lower altitude clouds (shown in Fig. 6). The histogram still shows a presence of higher altitude clouds, with an increasing proportion of low altitude clouds further from TSC-0. There is still a decreasing CTP at 5 days from convection.

Isolating just the high clouds using the ISCCP histograms, Fig. 7b shows a similar decline in the mean CTP, albeit at lower

255    pressures. The $\tau_c$ also sits at 200hPa initially, decaying to 250hPa in the first 6-12 hours as the convective core dissipates. The decay then slows, reaching 300hPa at 120 hours from convection.

Fig. 7c shows the evolution of the cloud optical thickness for all clouds. The all cloud $\tau_c$ drops significantly in the first 24 hours from convection, indicating the dissipation of the very thickest high clouds associated with the convective cores. This is to be expected as the regime shifts from thicker cirrus associated with convection, to thin cirrus that persists either after a

260    convective event, or is formed in situ and unrelated to convection.

When just looking at high clouds in Fig. 7d, the mean values of the histogram are relatively unchanged. However there is larger spread in the cloud optical thicknesses, including a relative increase in the optically thinnest of the clouds in the lowest bin.

### 3.4   Vertical profile evolution

265    The vertical distribution of cloud and $N_i$ vary strongly as a function of TSC. Fig. 8a shows the cloud amount and thus the general anvil shape of convective cores and their associated cirrus outflow up to 120 hours from convection. Fig. 8b shows the same up to 500 hours from convection. At very low TSC, there is a substantial amount of cloud at all altitudes up to approximately 16km associated with the very tops of the convective towers. At 1-2 hours since convection, the overshooting convective core is visible up to 18km. The low to mid altitude cloud, likely the convective cores, quickly dissipates as the TSC

270    increases. High clouds are maintained for much longer, with changes in the high cloud fraction continuing up to 120 hours from convection. There is a moderate amount of low clouds throughout the entire 120 hours since convection. There is also a sustained amount of mid level clouds between 4 and 8km for the first 60 hours. These mid level clouds are thought to form when latent heat associated with convective freezing creates a shallow temperature inversion which slows vertical motion in subsequent convective cycles and detrains moisture near the freezing level (Bourgeois et al., 2016). Fig. 8b shows that even at

275    very long TSC values, beyond 120 hours up to 500 hours, there is still a significant change in cloud amount as a function of TSC.

Fig. 8c shows the ice crystal number concentration for particles greater than $5\mu$m in diameter, $(N_i^5)$, as a function of the time since convection. Fig. 8e shows the same as Fig. 8c but for those greater than $100\mu$m, $(N_i^{100})$. Given that the $N_i$ is a very strong function of temperature (and therefore altitude), it is useful to consider the relative changes in the $N_i$ as a function of

280    TSC. Fig. 8d and 8e show the deviation of the $N_i$ to the tropical mean $N_i$ for a given altitude. Red indicates where the $N_i$ at a given TSC is greater than the tropical mean, and blue those regions where it is less than the tropical mean.
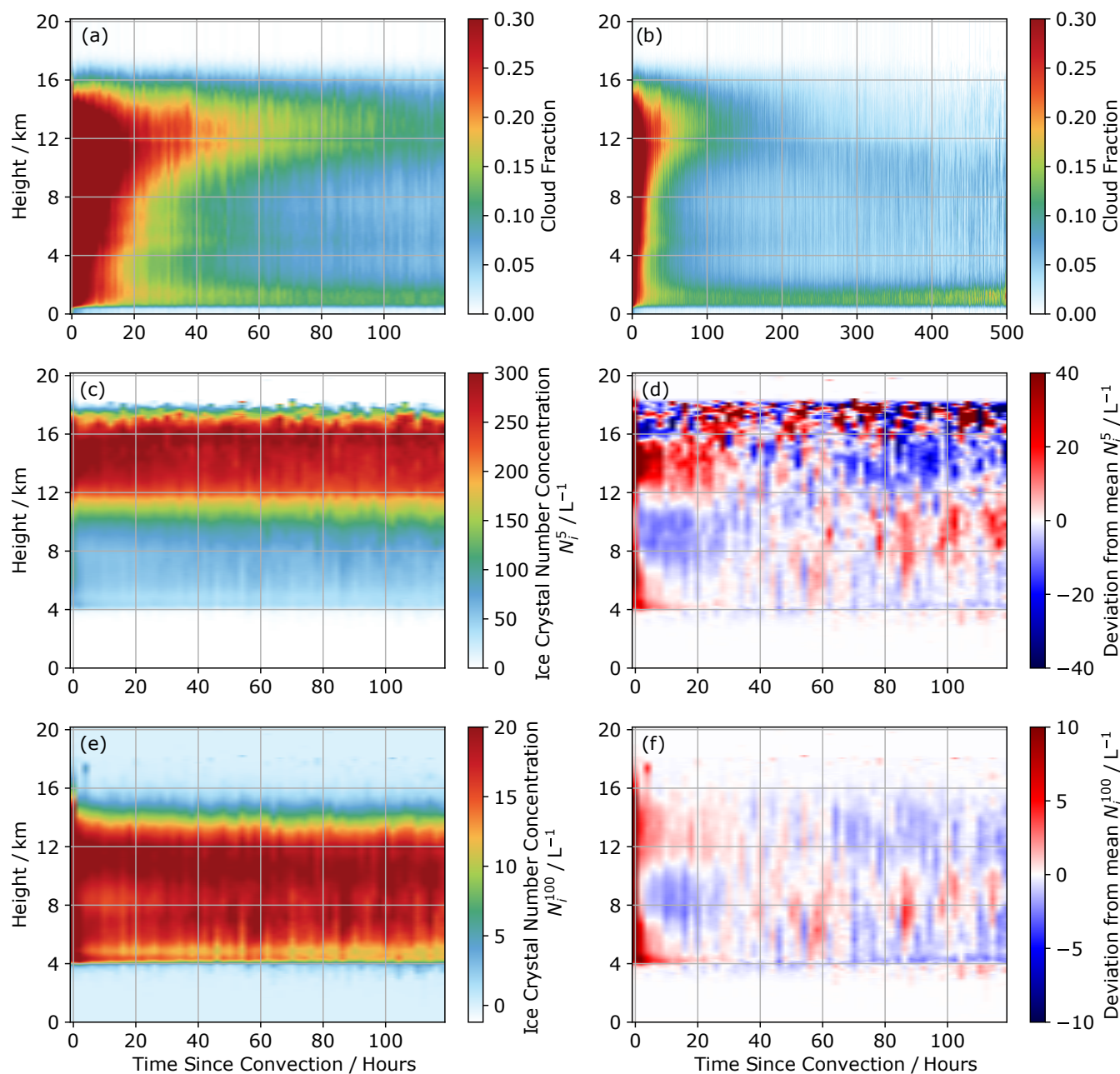
**Figure 8.** Vertical evolution of DARDAR cloud properties as a function of TSC. a) Cloud fraction up to 120 hours from convection. b) Cloud fraction up to 500 hours from convection. c) $N_i$ for particles larger than $5\mu$m. d) $N_i^5$ anomaly for 120 hours from convection. e) $N_i$ for particles larger than $5\mu$m. f) $N_i^{100}$ anomaly from mean value for 120 hours from convection. Anomaly here refers to the difference in the $N_i$ at a given TSC to the mean $N_i$ at that altitude for the tropics.

Considering Fig. 8d first, there is an greater than average $N_i^5$ at all altitudes close to convection. This is most notable between 12km and 16km, where the $N_i^5$ peaks. This is to be expected given the presence of a deep convective core. At short times after TSC-0, there remains an above average $N_i^5$ between 12km and 16km. This is indicative of the convective outflow that remains
285 after the convective core has dissipated. This outflow decays within 36-42 hours, when the deviation to the mean $N_i$ becomes negative. There is also an increase at similar times at lower latitudes between 4km and 8km that decays within around 20 hours. This is likely due to the active shallow convection that occurs close to the region of deep convection, and thin mid level clouds discussed in (Bourgeois et al., 2016). Considering Fig. 8f, there is a clear increase in the $N_i^{100}$ close to convection, particularly at lower altitudes between 4km and 8km. These larger ice crystals are expected in the convective core at lower altitudes as
290 they are less likely to be lifted higher into the cloud column as the smaller ice crystals, and also subside quicker (Jensen et al., 2018). The lower altitude $N_i$ drops off rapidly as the convective core dissipates. As in the case of the $N_i^5$, there is an increase in the $N_i^{100}$ between 12km and 16km which is sustained for the first 24 hours from convection and linked to updrafts of large ice crystals from deep convective cores.

## 3.5 Cloud radiative effects

295 The radiative evolution of convection, from thick convective core to thin anvil cirrus, is characterised by analysing the CERES SYN1deg L3 LW and SW TOA fluxes (NASA/LARC/SD/ASDC, 2017). Fig. 9 shows the SW, LW and net cloud radiative effect (CRE) as a function of the time since convection. Fig. 9a shows the evolution of the LW and SW and NET CRE for both the all cloud gridboxes, and high cloud only gridboxes, up to 500 hours from convection.

Fig. 9a shows that when considering the all cloud CRE, the net CRE is always slightly cooling, with an oscillation in the
300 first 48 hours due to the diurnal cycle in the CRE. This net CRE of close to zero in the tropics is well studied (Ramanathan et al., 1989; Hartmann and Berry, 2017; Wielicki et al., 1996). In the all cloud case, there is initially a very large significant warming and cooling that cancel each other out. The LW and SW CRE decreases significantly in the first 24-48 hours as the cloud fraction of these clouds drop. By 100 hours from convection there is very little change in the all cloud and high cloud CRE. To understand how the radiative forcing of the clouds that evolve from convection change, it is vital to consider only the
305 gridboxes containing high clouds.

The high CRE is a strong function of TSC at very low values of TSC (Fig. 9b). Initially, there is a large SW and LW component to the CRE, with -200Wm$^{-2}$ SW cooling and 150Wm$^{-2}$ LW warming at TSC-0, leading to a net CRE of -50Wm$^{-2}$ cooling. This is due to the very optically thick convective core that reflects a significant portion of the incoming solar radiation, whilst also having a very large LW warming due to its high cloud tops. As the convective core dissipates, and the
310 cloud optical thickness decreases, the SW CRE drops significantly, to 50Wm$^{-2}$ at 6 hours from convection, whereas the LW warming remains 90Wm$^{-2}$. At this point, the net CRE shifts from a cooling regime to a warming regime, dominated by the LW warming of the thinner detrained cirrus. After the initial dissipation of the core, the net warming is sustained. By 24 hours since convection, the net CRE remains at 90Wm$^{-2}$. By 120 hours from convection, the net CRE has decreased to 50Wm$^{-2}$. The histogram in Fig. 9b shows the LW warming splitting into two layers, with the weighted mean value falling in between. The
315 top layer, which sits at around 100Wm$^{-1}$ is the high cirrus with a high cloud fraction that has the largest warming potential.
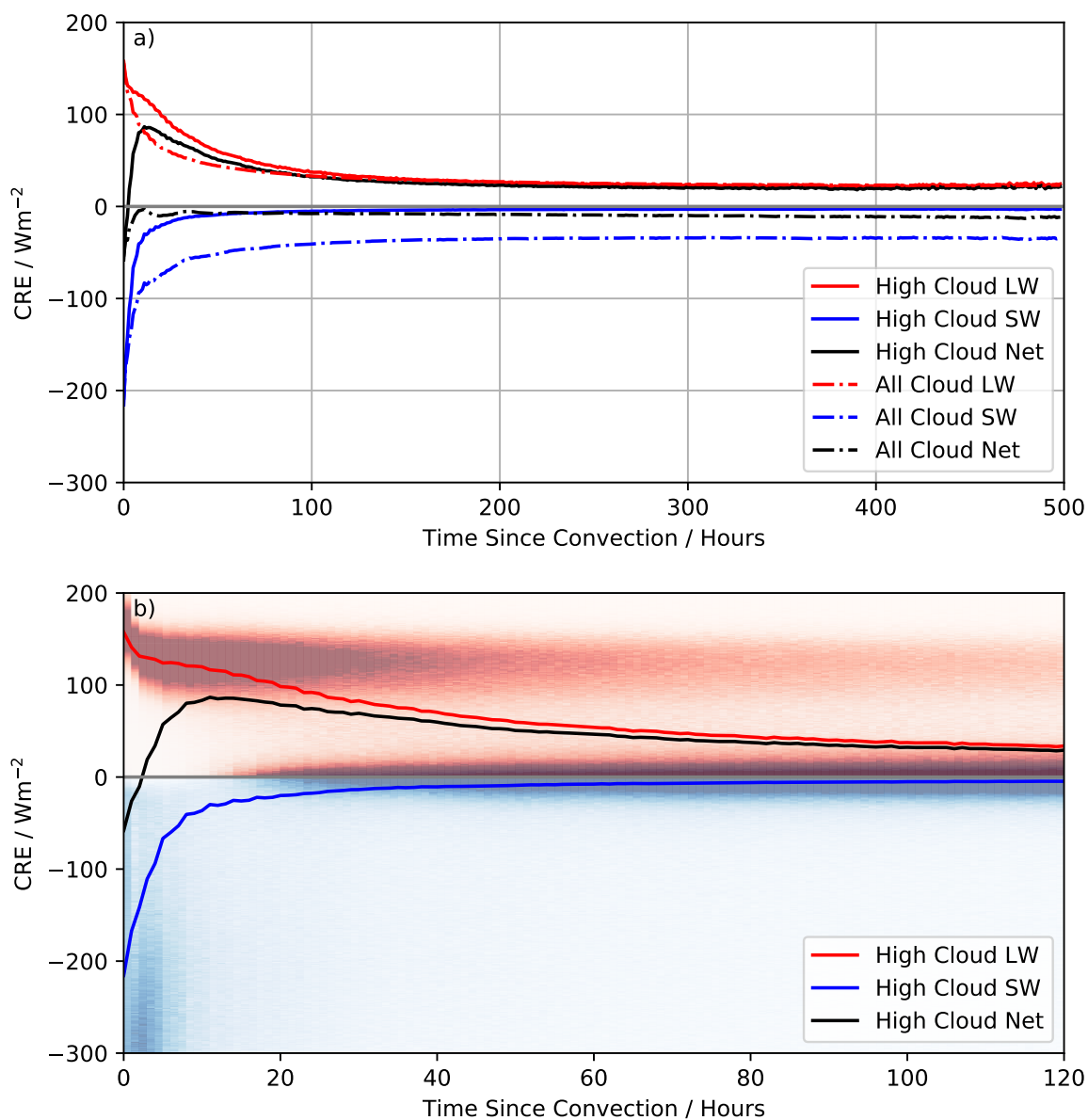
**Figure 9.** Cloud Radiative Effect (CRE) as a function of TSC. a) All cloud and high cloud LW, SW and Net CRE up to 500 hours from convection. b) High cloud only LW,SW and Net CRE up to 120 hours from convection with normalised joint histogram the showing the probability of finding a particular CRE value (LW in red, SW in blue) for a given TSC value.

The layer that emerges close to $0\mathrm{Wm}^{-2}$ is due to the lower cloud fraction high clouds that emerge further from convection. These clouds may be independent of convection, but occur nonetheless at longer times since convection. Because of their low cloud fraction, their CRE is small, and therefore sit along the $0\mathrm{Wm}^{-2}$ band in both the LW and SW.

This sustained warming as a function of TSC is not seen in previous studies. Gehlot and Quaas (2012) found the net CRE
320 in the ECHAM5 model to be negative up to five days (120 hours) from convection, however they did not isolate the high clouds, meaning that cooling from lower altitude thick clouds contributed to their CRE. Without removing low clouds from the analysis, the work in this paper finds a similar sustained, albeit small, cooling for the all cloud CRE (Fig. 9). Our results differ to previous model studies. Gasparini et al. (2021) looked at the CRE evolution, in E3SM, a high resolution GCM. These results found that, after an initial positive CRE due to small insolation values where convection occurred early before sunrise.
325 The SW and LW CRE quickly decayed, and the net CRE became negative after 2 hours, oscillating to a small warming again at 15 hours as the solar insolation decreased. These simulations do not represent the thinnest cirrus particularly well, so may underestimate some of the LW warming seen in this work.

## 4 Discussion

There are multiple benefits to the approach highlighted in this paper. It is computationally efficient when compared to tracking
330 every single location of deep convection in the tropics. Instead of keeping and updating an array of locations for each new convective event, which grows with each timestep, this work has just one TSC array for the entire tropics, which is updated at each timestep. It also removes any bias in selecting specific convection, since all convection from the shortest lived to the longest lived contribute to the mean TSC. Finally, the unbounded nature of the tracking means that the full life cycle of all convection is considered, until it is superseded by new convection.
335 However, there are some uncertainties introduced in the TSC algorithm. Firstly, it only considers horizontal wind fields, averaged between 200-300hPa, and there is no vertical advection of the TSC. This is a similar assumption as made by Luo and Rossow (2004), except that they considered a larger pressure averaged wind field between 200-500hPa. The choice of the 200-300hPa average wind field is supported by the evolution of the ISCCP CTP (Fig. 7), and the evolution of the HYSPLIT trajectory pressures. There is some vertical subsidence during the evolution of the cirrus, therefore using the 200-300hPa wind
340 field means there is some uncertainty in the advection of the air from deep convection. Adding a vertical component would be an option for future enhancement to the TSC algorithm. It would add considerable computational complexity, but would improve the calculations of TSC and reduce uncertainty introduced by using a pressure averaged wind field.

Secondly, there is necessary interpolation that occurs when the wind field diverges. If a grid box becomes empty between timesteps, then the value for the TSC in that grid box is calculated as the mean value of the surrounding grid boxes. This
345 increases the uncertainty in longer TSC values.

Some key assumptions were made when investigating the evolution of the CRE as a function of the TSC. Firstly, when there is missing data in the LW clear sky values, these gridboxes are filled with the 3 monthly seasonal mean LW clear sky values. The monthly mean was considered, however it still contained NaN values in certain months. It is important to fill in this

missing data, as the locations where there are no LW clear sky values correlate strongly to the regions close to convection in
350   the tropics, and leaving this missing data in the analysis would mean that there are fewer LW CRE values close to convection.

Secondly, the use of the ISCCP dataset to isolate the high cloud CRE was only possible during daylight hours, as the ISCCP
joint histograms were only available during daylight. The SW CRE at night was known to be zero so could be filled in for
the high cloud CRE. However, the high cloud LW CRE is not available at night and therefore not included in the analysis.
"implicitly assumes" The implication of this is that we have assumed the nighttime LW CRE values to not differ greatly to
355   the daytime LW CRE values. It would be possible to account for the missing data in future work by using a radiative transfer
model to explicitly calculate the nighttime CRE values (L'Ecuyer et al., 2008).

## 5   Conclusion

The lifecycle of convective cores and their associated anvil cirrus outflows, including their vertical evolution, have been char-
acterised in this paper through the creation of a 'Time Since Convection (TSC)' dataset. This has allowed for the investigation
360   of the radiative evolution of convection to be explained through changes in cloud properties. The convection was identified
(Fig. 1), and then advected in a wind field to generate the TSC dataset in Fig. 4. This allows an unbounded upper limit for
the time since convection, in contrast to previous studies that tracked individual trajectories and were forced to set an artificial
limit to their length (Luo and Rossow, 2004; Gehlot and Quaas, 2012).

In particular, changes in the high cloud-only fields were found to differ significantly from the all-cloud fields. Isolating just
365   the high clouds is particularly useful as it enables analysis of the CRE of detrained cirrus alone, which showed significant
differences to the all-cloud CRE. The general trend for high altitude, optically thinner clouds that is expected in the evolution
of deep convection to anvil to thin cirrus is visible in Fig. 7. There is a sharp initial decay in both the CTP and COT in the first
12 hours from convection, before decreasing more slowly over the next 120 hours.

Characterising the vertical evolution of cloudiness shows the thinning of the anvil over time (Figs. 8a,b), with changes
370   still visible at TSC>120 hours. These results also show an initial vertical growth stage at very short TSC, associated with
overshooting convective cores.

The changes in cloud properties explain the observed evolution of the CRE as a function of TSC shown in Fig. 9. In the all
cloud CRE case, the net CRE oscillates very close to zero for all values of TSC. This apparent balance in the tropical CRE
is well documented (Wielicki et al., 1996; Ramanathan et al., 1989; Hartmann and Berry, 2017), and occurs even close to
375   convection when the the LW and SW values are very high. However, when the high cloud only regions are isolated, there is
a sustained warming beyond 120 hours from convection after a brief initial cooling. This difference is predominantly due to
changes in the SW cooling between the all cloud and high cloud cases. As shown in Fig. 7, there is an increasing contribution of
low clouds to the mean CTP further from convection. When low clouds are removed, the SW cooling is substantially reduced,
as all that remains is optically thinner high clouds (Fig. 9b). The LW warming from the optically thin high clouds is sustained
380   beyond 24 hours from convection, by which point the strong SW cooling effect of the convective cores has dissipated (Fig.
9b). This work has highlighted the large values of of the LW and SW CRE close to convection for high clouds. Investigating

the factors controlling the radiative balance between this warming and cooling is important, as small changes in the cloud properties could potentially have a significant effect on the net CRE due to small changes in these large values.

385 This paper has introduced a novel method for calculating the time since convection from deep convection, through anvil cirrus to thin cirrus. This method improves on prior work by being able to track air from convection for unbounded lengths at low computational costs, and accounting for intersections and overlaps of convection. Using this method, the evolution of the radiative properties, and the microphysical controls on the convective regimes have been investigated. Whilst there are significant changes in CRE found close to convection, this work also also demonstrates that changes are present in cloud properties at timescales up to 500 hours from convection, long after the convection has dissipated, signalling the need for
390 further study at these timescales.

*Author contributions.* Both authors contributed to study design and interpretation of results. GH performed the analysis and prepared the manuscript, with comments from EG.

*Competing interests.* The contact author has declared that neither they nor their co-author has any competing interests.

*Acknowledgements.* This work was supported by a Royal Society University Research Fellowship (URF\R1\191602) and a PhD studentship
395 from the Department of Physics, Imperial College London. The authors gratefully acknowledge the NOAA Air Resources Laboratory (ARL) for the provision of the HYSPLIT transport and dispersion model and READY website (https://www.ready.noaa.gov) used in this publication. The authors also gratefully acknowledge Odran Sourdeval and Athulya Saiprakash at the University of Lille for providing the DARDAR data, and for helpful discussions and suggestions.

# References

400 Berry, E. and Mace, G. G.: Cloud properties and radiative effects of the Asian summer monsoon derived from A-Train data, Journal of Geophysical Research: Atmospheres, 119, 9492–9508, https://doi.org/10.1002/2014JD021458, 2014.

Bourgeois, Q., Ekman, A. M. L., Igel, M. R., and Krejci, R.: Ubiquity and impact of thin mid-level clouds in the tropics, Nature Communications, 7, 12 432, https://doi.org/10.1038/ncomms12432, 2016.

Choi, Y.-S. and Ho, C.-H.: Radiative effect of cirrus with different optical properties over the tropics in MODIS and CERES observations, 405 Geophysical Research Letters, 33, https://doi.org/10.1029/2006GL027403, 2006.

Delanoë, J. and Hogan, R. J.: A variational scheme for retrieving ice cloud properties from combined radar, lidar, and infrared radiometer, Journal of Geophysical Research: Atmospheres, 113, https://doi.org/10.1029/2007JD009000, 2008.

Fan, J., Leung, L. R., Rosenfeld, D., Chen, Q., Li, Z., Zhang, J., and Yan, H.: Microphysical effects determine macrophysical response for aerosol impacts on deep convective clouds, Proceedings of the National Academy of Sciences, 110, E4581–E4590, 410 https://doi.org/10.1073/pnas.1316830110, 2013.

Garrett, T. J., Navarro, B. C., Twohy, C. H., Jensen, E. J., Baumgardner, D. G., Bui, P. T., Gerber, H., Herman, R. L., Heymsfield, A. J., Lawson, P., Minnis, P., Nguyen, L., Poellot, M., Pope, S. K., Valero, F. P. J., and Weinstock, E. M.: Evolution of a Florida Cirrus Anvil, Journal of the Atmospheric Sciences, 62, 2352 – 2372, https://doi.org/10.1175/JAS3495.1, 2005.

Gasparini, B., Blossey, P. N., Hartmann, D. L., Lin, G., and Fan, J.: What Drives the Life Cycle of Tropical Anvil Clouds?, Journal of 415 Advances in Modeling Earth Systems, 11, 2586–2605, https://doi.org/10.1029/2019MS001736, 2019.

Gasparini, B., Rasch, P. J., Hartmann, D. L., Wall, C. J., and Dütsch, M.: A Lagrangian Perspective on Tropical Anvil Cloud Lifecycle in Present and Future Climate, Journal of Geophysical Research: Atmospheres, 126, e2020JD033 487, https://doi.org/10.1029/2020JD033487, e2020JD033487 2020JD033487, 2021.

Gehlot, S. and Quaas, J.: Convection-Climate Feedbacks in the ECHAM5 General Circulation Model: Evaluation of Cirrus Cloud Life Cycles 420 with ISCCP Satellite Data from a Lagrangian Trajectory Perspective, Journal of Climate, 25, 5241 – 5259, https://doi.org/10.1175/JCLI-D-11-00345.1, 2012.

Harrison, E. F., Minnis, P., Barkstrom, B. R., Ramanathan, V., Cess, R. D., and Gibson, G. G.: Seasonal variation of cloud radiative forcing derived from the Earth Radiation Budget Experiment, Journal of Geophysical Research: Atmospheres, 95, 18 687–18 703, https://doi.org/10.1029/JD095iD11p18687, 1990.

425 Hartmann, D. L. and Berry, S. E.: The balanced radiative effect of tropical anvil clouds, Journal of Geophysical Research: Atmospheres, 122, 5003–5020, https://doi.org/10.1002/2017JD026460, 2017.

Hartmann, D. L., Holton, J. R., and Fu, Q.: The heat balance of the tropical tropopause, cirrus, and stratospheric dehydration, Geophysical Research Letters, 28, 1969–1972, https://doi.org/10.1029/2000GL012833, 2001a.

Hartmann, D. L., Moy, L. A., and Fu, Q.: Tropical Convection and the Energy Balance at the Top of the Atmosphere, Journal of Climate, 14, 430 4495 – 4511, https://doi.org/10.1175/1520-0442(2001)014<4495:TCATEB>2.0.CO;2, 2001b.

Hersbach, H., Bell, B., Berrisford, P., Biavati, G., Horányi, A., Muñoz Sabater, J., Nicolas, J., Peubey, C., Radu, R., Rozum, I., Schepers, D., Simmons, A., Soci, C., Dee, D., and Thépaut, J.-N.: ERA5 hourly data on pressure levels from 1959 to present., https://doi.org/10.24381/cds.bd0915c6, 2018.

Jensen, E. J., van den Heever, S. C., and Grant, L. D.: The Life Cycles of Ice Crystals Detrained From the Tops of Deep Convection, Journal 435 of Geophysical Research: Atmospheres, 123, 9624–9634, https://doi.org/10.1029/2018JD028832, 2018.

Kiehl, J. T.: On the Observed Near Cancellation between Longwave and Shortwave Cloud Forcing in Tropical Regions, Journal of Climate, 7, 559–565, https://doi.org/10.1175/1520-0442(1994)007<0559:OTONCB>2.0.CO;2, 1994.

Koren, I., Remer, L. A., Altaratz, O., Martins, J. V., and Davidi, A.: Aerosol-induced changes of convective cloud anvils produce strong climate warming, Atmospheric Chemistry and Physics, 10, 5001–5010, https://doi.org/10.5194/acp-10-5001-2010, 2010.

440 Krämer, M., Rolf, C., Luebke, A., Afchine, A., Spelten, N., Costa, A., Meyer, J., Zöger, M., Smith, J., Herman, R. L., Buchholz, B., Ebert, V., Baumgardner, D., Borrmann, S., Klingebiel, M., and Avallone, L.: A microphysics guide to cirrus clouds – Part 1: Cirrus types, Atmospheric Chemistry and Physics, 16, 3463–3483, https://doi.org/10.5194/acp-16-3463-2016, 2016.

Luo, Z. and Rossow, W. B.: Characterizing Tropical Cirrus Life Cycle, Evolution, and Interaction with Upper-Tropospheric Water Vapor Using Lagrangian Trajectory Analysis of Satellite Observations, Journal of Climate, 17, 4541 – 4563, https://doi.org/10.1175/3222.1, 445 2004.

L'Ecuyer, T. S., Wood, N. B., Haladay, T., Stephens, G. L., and Stackhouse, P. W.: Impact of clouds on atmospheric heating based on the R04 CloudSat fluxes and heating rates data set, Journal of Geophysical Research: Atmospheres, 113, https://onlinelibrary.wiley.com/doi/abs/10.1029/2008JD009951, 2008.

Mace, G. G., Deng, M., Soden, B., and Zipser, E.: Association of Tropical Cirrus in the 10–15-km Layer with Deep Convective Sources: 450 An Observational Study Combining Millimeter Radar Data and Satellite-Derived Trajectories, Journal of the Atmospheric Sciences, 63, 480–503, https://doi.org/10.1175/JAS3627.1, 2006.

Massie, S., Gettelman, A., Randel, W., and Baumgardner, D.: Distribution of tropical cirrus in relation to convection, Journal of Geophysical Research: Atmospheres, 107, AAC 19–1–AAC 19–16, https://doi.org/10.1029/2001JD001293, 2002.

NASA/LARC/SD/ASDC: CERES and GEO-Enhanced TOA, Within-Atmosphere and Surface Fluxes, Clouds and Aerosols 1-Hourly Terra- 455 Aqua Edition4A, 10.5067/TERRA+AQUA/CERES/SYN1DEG-1HOUR_L3.004A, 2017.

Pincus, R., Platnick, S., Ackerman, S. A., Hemler, R. S., and Hofmann, R. J. P.: Reconciling Simulated and Observed Views of Clouds: MODIS, ISCCP, and the Limits of Instrument Simulators, Journal of Climate, 25, 4699 – 4720, https://doi.org/10.1175/JCLI-D-11-00267.1, 2012.

Protopapadaki, S. E., Stubenrauch, C. J., and Feofilov, A. G.: Upper tropospheric cloud systems derived from IR sounders: properties of 460 cirrus anvils in the tropics, Atmospheric Chemistry and Physics, 17, 3845–3859, https://doi.org/10.5194/acp-17-3845-2017, 2017.

Ramanathan, V., Cess, R. D., Harrison, E. F., Minnis, P., Barkstrom, B. R., Ahmad, E., and Hartmann, D.: Cloud-Radiative Forcing and Climate: Results from the Earth Radiation Budget Experiment, Science, 243, 57–63, https://doi.org/10.1126/science.243.4887.57, 1989.

Riihimaki, L. D., McFarlane, S. A., Liang, C., Massie, S. T., Beagley, N., and Toth, T. D.: Comparison of methods to determine Tropical Tropopause Layer cirrus formation mechanisms, Journal of Geophysical Research: Atmospheres, 117, 465 https://doi.org/10.1029/2011JD016832, 2012.

Rolph, G., Stein, A., and Stunder, B.: Real-time Environmental Applications and Display sYstem: READY, Environmental Modelling and Software, 95, 210–228, https://doi.org/10.1016/j.envsoft.2017.06.025, 2017.

Rossow, W., Golea, V., Walker, A., Knapp, K., Young, A., Hankins, B., and Inamdar, A.: International Satellite Cloud Climatology Project (ISCCP) Climate Data Record, H-Series, https://doi.org/10.7289/V5QZ281S, 2017.

470 Salathé, E. P. and Hartmann, D. L.: A Trajectory Analysis of Tropical Upper-Tropospheric Moisture and Convection, Journal of Climate, 10, 2533–2547, http://www.jstor.org/stable/26243410, 1997.

Sourdeval, O., Gryspeerdt, E., Krämer, M., Goren, T., Delanoë, J., Afchine, A., Hemmer, F., and Quaas, J.: Ice crystal number concentration estimates from lidar–radar satellite remote sensing – Part 1: Method and evaluation, Atmospheric Chemistry and Physics, 18, 14 327–14 350, https://doi.org/10.5194/acp-18-14327-2018, 2018.

475 Tselioudis, G., Rossow, W. B., Jakob, C., Remillard, J., Tropf, D., and Zhang, Y.: Evaluation of Clouds, Radiation, and Precipitation in CMIP6 Models Using Global Weather States Derived from ISCCP-H Cloud Property Data, Journal of Climate, 34, 7311 – 7324, https://doi.org/10.1175/JCLI-D-21-0076.1, 2021.

Wall, C. J. and Hartmann, D. L.: Balanced Cloud Radiative Effects Across a Range of Dynamical Conditions Over the Tropical West Pacific, Geophysical Research Letters, 45, 11,490–11,498, https://doi.org/10.1029/2018GL080046, 2018.

480 Wall, C. J., Hartmann, D. L., Thieman, M. M., Smith, W. L., and Minnis, P.: The lifecycle of anvil clouds and the top-of-atmosphere radiation balance over the tropical west Pacific, Journal of climate, 31, 10 059–10 080, https://doi.org/10.1175/jcli-d-18-0154.1, 2018.

Wielicki, B. A., Barkstrom, B. R., Harrison, E. F., Lee, R. B., Smith, G. L., and Cooper, J. E.: Clouds and the Earth's Radiant Energy System (CERES): An Earth Observing System Experiment, Bulletin of the American Meteorological Society, 77, 853–868, https://doi.org/10.1175/1520-0477(1996)077<0853:CATERE>2.0.CO;2, 1996.